Breast Cancer: Targets and Therapy

Dovepress
Taylor & Francis Group

Open Access Full Text Article

ORIGINAL RESEARCH

Ki-67 Prediction in Breast Cancer: Integrating Radiomics From Automated Breast Volume Scanner and 2D Ultrasound Images via Machine Learning

Wei Wei[1,2,*], Fei Xia[3,*], Wang Zhou[1,*], Wenwu Lu[1], Di Zhang[1], Qianqing Ma[2], Xiangyi Xu[1], Chaoxue Zhang[1]

[1]Department of Ultrasound, The First Affiliated Hospital of Anhui Medical University, Hefei, Anhui, People's Republic of China; [2]Department of Ultrasound, The First Affiliated Hospital of Wannan Medical College (Yijishan Hospital), Wuhu, People's Republic of China; [3]Department of Ultrasound, WuHu Hospital, East China Normal University (The Second People's Hospital, WuHu), Wuhu, Anhui, People's Republic of China

*These authors contributed equally to this work

Correspondence: Chaoxue Zhang, Department of Ultrasound, The First Affiliated Hospital of Anhui Medical University, No. 218 Jixi Road, Shushan District, Hefei, Anhui, People's Republic of China, Email zcxay@163.com

Breast Cancer: Targets and Therapy downloaded from https://www.dovepress.com/
For personal use only.

Purpose: This study aimed to develop and validate a predictive model using radiomics features from automatic breast volume scanner (ABVS) and 2D ultrasound images to preoperatively assess Ki-67 expression in breast cancer (BC), thereby supporting personalized clinical treatment planning.

Methods: Data from 426 BC patients who met the inclusion criteria were retrospectively analyzed. Univariate and multivariate logistic regression analyses were performed on the clinical ultrasound characteristics to construct a clinical model. Radiomics features were extracted from both the tumor and the sub-regions based on ABVS and 2D images. The silhouette coefficient was used to evaluate clustering performance and determine the optimal number of clusters. Radiomics-based prediction models were developed using four machine learning classifiers: Logistic Regression, ExtraTree, XGBoost, and LightGBM. A combined model was further constructed by integrating radiomics and habitat radiomics features from ABVS and 2D images with relevant clinical factors. Model performance was evaluated using the Receiver Operating Characteristic (ROC) curve, calibration curve, and decision curve analysis (DCA).

Results: In the validation set, the area under the ROC curve (AUC) values of the radiomics model ($Rad_{ABVS\ +\ 2D}$), the habitat radiomics model ($Hab_{ABVS\ +\ 2D}$), and the combined radiomics model ($Rad\text{-}Hab_{ABVS\ +\ 2D}$) were 0.603, 0.664, and 0.850, respectively. By integrating independent clinical factors (US-ALNs, T-stage) with the $Rad\text{-}Hab_{ABVS\ +\ 2D}$ model, a comprehensive model ($CM_{Clinical\ +\ Rad\text{-}Hab}$) was constructed using LightGBM. According to the DeLong test, this model significantly outperformed others in terms of AUC ($P < 0.05$). The AUC values for the training and validation sets were 0.951 (95% CI: 0.928–0.973) and 0.884 (95% CI: 0.832–0.949), respectively. The calibration curves and DCA of $CM_{Clinical\ +\ Rad\text{-}Hab}$ demonstrated excellent model calibration and clinical utility.

Conclusion: The $CM_{Clinical\ +\ Rad\text{-}Hab}$ model developed in this study enables accurate preoperative prediction of *Ki-67* expression in BC patients, facilitating personalized and precise treatment strategies.

Keywords: breast cancer, *Ki-67*, automated breast volume scanner, radiomics, ultrasound

Introduction

Breast cancer (BC) has become the most commonly diagnosed cancer and remains a leading cause of cancer-related mortality among women worldwide.[1] *Ki-67*, a nuclear protein associated with cellular proliferation, serves as an essential marker for evaluating tumor growth dynamics.[2] Elevated *Ki-67* expression is associated with an increased risk of tumor invasion and recurrence.[3] Moreover, it correlates with the pathological complete response rate to neoadjuvant therapy (NAT) in BC patients.[4] A study by Chen et al found that higher pre-treatment *Ki-67* levels were associated with a better clinical response to neoadjuvant chemotherapy in luminal BC subtypes. Specifically, a *Ki-67* cutoff value of 25.5% was identified as a predictor of treatment

Received: 3 June 2025
Accepted: 4 September 2025
Published: 11 October 2025

© 2025 Wei et al. This work is published and licensed by Dove Medical Press Limited. The full terms of this license are available at https://www.dovepress.com/terms.php and incorporate the Creative Commons Attribution – Non Commercial (unported, v4.0) License (http://creativecommons.org/licenses/by-nc/4.0/). By accessing the work you hereby accept the Terms. Non-commercial uses of the work are permitted without any further permission from Dove Medical Press Limited, provided the work is properly attributed. For permission for commercial use of this work, please see paragraphs 4.2 and 5 of our Terms (https://www.dovepress.com/terms.php).

response, indicating that *Ki-67* could serve as a valuable biomarker for guiding individualized treatment strategies.[5] Furthermore, the POETIC trial demonstrated that changes in *Ki-67* levels during preoperative endocrine therapy were predictive of long-term outcomes, underscoring the critical role of *Ki-67* in informing treatment strategies and optimizing patient management.[6] Currently, *Ki-67* expression is assessed via immunohistochemical (IHC) analysis, which typically requires an invasive core needle biopsy (CNB) prior to surgery. However, due to intratumoral heterogeneity and the limited sampling of CNB, discrepancies between CNB and postoperative specimens are frequently observed, with reported inconsistency rates ranging from 10% to 40%.[7] Therefore, there is a pressing need for an accurate, comprehensive, and non-invasive method to predict preoperative *Ki-67* expression, which is essential for clinical decision-making.

Ultrasound (US) is widely used for the diagnosis of BC due to its simplicity, low cost, and non-invasive nature.[8] Compared to conventional US, ABVS enhances reproducibility through automated scanning,[9] representing a significant technological advancement in US imaging.[10] Its standardized coronal imaging offers detailed lesion information, making it particularly suitable for radiomics analysis.[11] Radiomics enables the extraction of high-throughput quantitative features from medical images, allowing for a comprehensive characterization of tumor phenotype.[12] It has been increasingly applied in tumor diagnosis, treatment planning, and prognosis prediction.[13] The significant potential of radiomics has been fully demonstrated across numerous oncology applications, particularly in improving the predictive performance of ABVS in BC management.[11,14–17] This progress marks a major step toward non-invasive tumor biological profiling and further integrates medical imaging with personalized medicine.[18] However, tumor heterogeneity, arising from variations in cell composition and spatial distribution, poses a challenge to accurate characterization.[19] To better visualize and quantify this heterogeneity, voxel clusters with similar tumor biological characteristics can be grouped into sub-regions.[20] Habitat radiomics, an emerging approach, segments tumors into biologically similar sub-regions and extracts features from these areas to enhance the assessment of tumor heterogeneity. A recent study,[21] involving multi-modal logistic regression models based on magnetic resonance imaging (MRI), US, and mammography revealed that incorporating peripheral tumor features (within 5 mm) yielded the best performance in distinguishing benign from malignant breast nodules, with an AUC of 0.905 (95% CI: 0.805–1). This highlights the increasing value of multimodal radiomics approaches. Previous US-based radiomics studies have shown promise in predicting *Ki-67* expression in BC.[16,17] However, these studies were limited by small sample sizes and single-modality imaging, which may not fully capture the complex characteristics of tumors. Additionally, habitat radiomics has not been widely explored in this context. As tumor heterogeneity plays a crucial role in understanding tumor biology, habitat radiomics may enhance predictive accuracy. To address these limitations, our study integrates multimodal radiomics derived from ABVS and 2D US, along with habitat radiomics, to provide a more comprehensive and accurate prediction of *Ki-67* expression in BC.

Motivated by these insights, we aim to evaluate the predictive value of radiomics and habitat radiomics features, captured from entire tumors and their sub-regions, using a machine learning (ML) model. Our goal is to establish a robust, non-invasive model for predicting *Ki-67* expression in BC, thereby supporting personalized treatment strategies and improving prognostic assessment.

Materials and Methods

Study Population

This retrospective study was conducted in accordance with the Declaration of Helsinki and was approved by the Ethics Committee of the First Affiliated Hospital of Anhui Medical University (Approval No. PJ2023-07-11). Given the retrospective nature of the study, which involved the use of previously collected cases and medical records without any new clinical interventions, the requirement for informed consent was waived in accordance with relevant ethical guidelines. To ensure data reliability, strict inclusion and exclusion criteria were applied. The inclusion criteria were as follows: (1) Patients pathologically diagnosed with BC who underwent both ABVS and conventional US examinations within two weeks prior to surgery; (2) No NAT administered before surgery; (3) Availability of complete clinical and pathological information. The exclusion criteria were: (1) Incomplete clinical or pathological data; (2) History of other malignant tumors; (3) Receipt of preoperative NAT; (4) Maximum tumor diameter > 50 mm as measured by US; (5) Presence of bilateral BC. A total of 426 patients with BC met the eligibility criteria. The cases were randomly divided into a training set (n = 297) and a validation set (n = 127), following a 7:3 ratio (Figure 1).

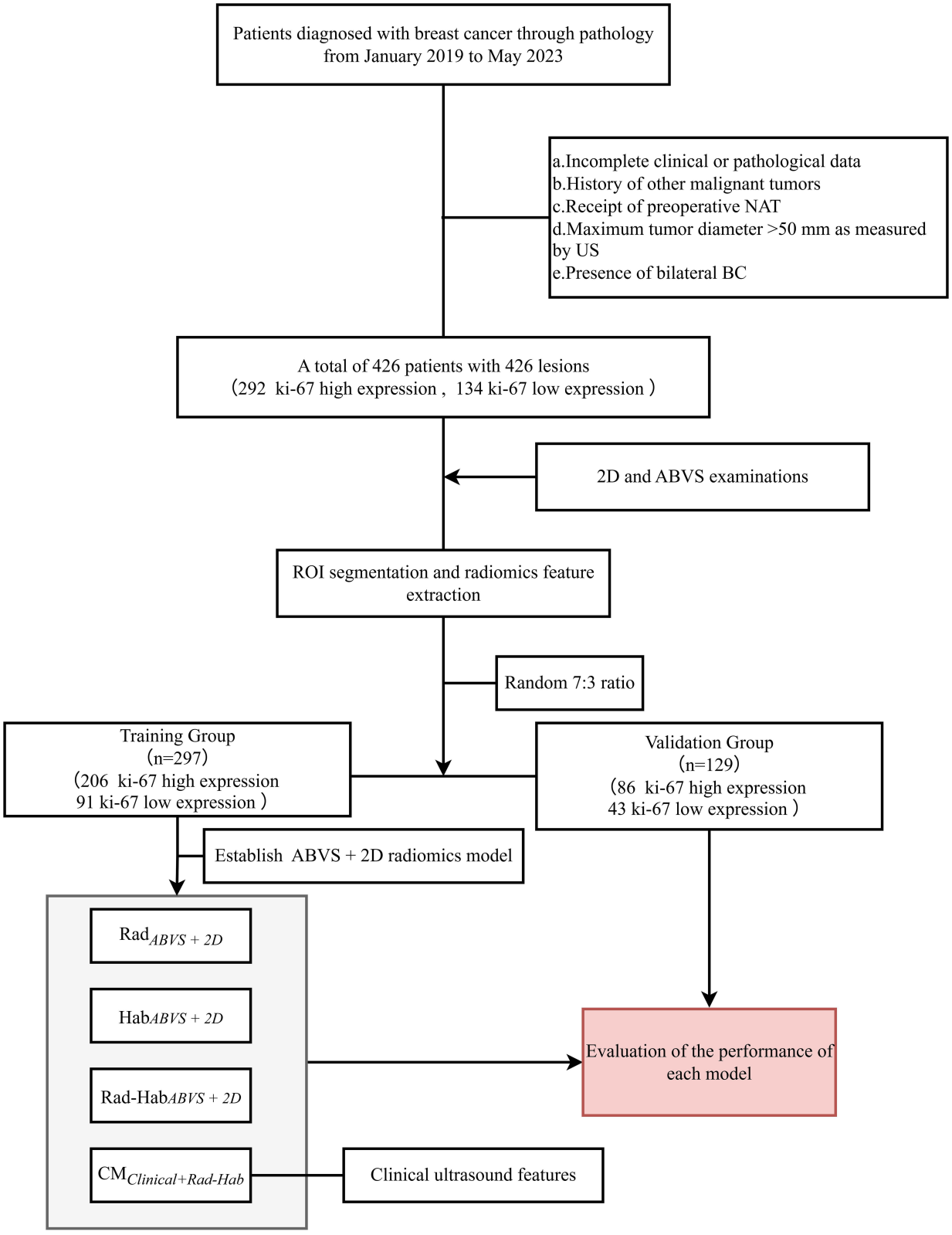

Figure 1 Flowchart of the entire research.

Abbreviations: ROI, Region of Interest; ABVS, automated breast volume scanner; Rad$_{ABVS+2D}$, Radiomics ABVS and 2D model; Had$_{ABVS+2D}$, Habitat radiomics ABVS and 2D model; Rad-Hab$_{ABVS+2D}$, Radiomics and Habitat radiomics ABVS and 2D model; CM$_{Clinical\ +\ Rad-Hab}$, Clinical–Radiomics–Habitat $_{ABVS+2D}$ Combined Model.

https://doi.org/10.2147/BCTT.S540595

Clinical and Histopathological Data Acquisition and Assessment

Details regarding image acquisition, evaluation procedures, and US equipment specifications are provided in Supplementary Material S1. Breast lesion classification was performed according to the fifth edition of the American College of Radiology (ACR) Breast Imaging Reporting and Data System (BI-RADS).[22] The *Ki-67* proliferation index was calculated based on the percentage of malignant cells showing positive nuclear staining for *Ki-67*. A *Ki-67* score ≥ 20% was defined as high expression, while a score < 20% was considered low expression.[23,24]

Segmentation of Regions of Interest (ROIs) and Generation of Habitat Sub-Regions

To segment the lesion regions on ABVS coronal images and 2D US images, the ITK-SNAP software (version 3.8, website: www.itk-snap.org) was used for tumor segmentation. Details of the tumor ROI delineation process are provided in Supplementary Material S2. Before generating habitat sub-regions, the tumors were first localized on both ABVS and 2D images. Each image was paired with a tumor mask of identical dimensions. The bounding box of the tumor region was extracted from the corresponding mask file, and this region was used to define the area for further analysis. Radiomic features were then extracted from these sub-regions. For each pixel within the tumor, a 5 × 5×5 sliding window was applied, expanding outward by two pixels in each direction. Radiomic features within this window were extracted using the pyradiomics library. To enable subsequent clustering analysis, all features were normalized to a range of 0 to 1. This standardization mitigates the influence of features with larger numerical scales and enhances the accuracy and robustness of clustering.[25]

Although larger windows and a greater number of features may improve robustness to noise, they also significantly increase computational complexity, especially when extracting features at the pixel level. Therefore, in this study, the number of radiomic features was limited to five, specifically those derived from the Gray-Level Co-occurrence Matrix (GLCM). The GLCM effectively captures subtle textural variations in the image, reflecting microscopic irregularity and complexity. It has been widely used to reveal the potential relationship between tumor tissue structure and biological behavior, making it an important tool in the study of tumor heterogeneity[25,26] Subsequently, to further quantify image data, each pixel's local histological features were transformed into a five-dimensional feature vector. This vector integrates multiple aspects of local feature information, such as texture, contrast, and uniformity, facilitating subsequent quantitative analysis and model construction.

A Gaussian mixture model (GMM) clustering algorithm was employed to identify tumor sub-regions composed of biologically similar pixels. Clustering was performed at the cohort level, rather than the individual patient level, to ensure consistent cluster assignment across patients and to allow the propagation of cluster centers from the training set to the test set, ensuring consistent clustering during model application. To determine the optimal number of clusters (ie, habitats), the Silhouette coefficient was used to evaluate clustering performance across a range of k values from 2 to 10. Following clustering, each cluster was assigned a unique color label to generate a cluster label map, which reflected the global distribution of internal regions within the tumor.

Radiomics Feature Extraction

Radiomics features were extracted from both tumor regions and sub-regions within the ABVS and 2D US images. Prior to feature extraction, image preprocessing was performed to ensure consistency across datasets. First, the signal intensity of the original images was normalized and standardized to a range of 0–100 to minimize intensity variations between images. Next, spatial resampling was conducted to achieve a uniform in-plane pixel resolution of 2 mm in the XY direction. All feature extraction was confined to the two-dimensional plane. Image gray levels were discretized based on a predefined bin width (eg, grouping every 5 intensity values), enabling standardized texture quantification. All processing was applied exclusively to regions defined by the specified labels in the tumor mask. A wavelet filter was used for feature enhancement prior to extraction. Radiomics features were extracted using the open-source Python package PyRadiomics (https://pyradiomics.readthedocs.io/en/latest/index.html, version 3.0.1), developed by the Computational Imaging Bioinformatics Laboratory at Harvard Medical School. Both unfiltered (from original images) and filtered features were included in the analysis. A total of 464 features were extracted and categorized into the following classes: 90 first-order features, 9 shape features, 110 Gray-Level Co-occurrence Matrix (GLCM) features, 80 gray-level size zone matrix (GLSZM) features, 80 gray-level run length matrix (GLRLM) features, 25 neighboring gray-tone difference matrix (NGTDM) features, 70 gray-level dependence matrix (GLDM) features.

PyRadiomics adheres to the standards of the Imaging Biomarker Standardization Initiative (IBSI), ensuring consistent definitions and methodologies for radiomic feature extraction.

Radiomics Feature Selection

The selection of predictive features associated with *Ki-67* expression was performed through a multi-step process. This included screening radiomics features, sub-regional radiomics features, and clinical US features. The detailed feature selection workflow is presented in Supplementary Material S3.

Construction and Validation of ML Models

After feature selection and fusion, five predictive models were developed, namely the clinical model, the radiomics model (Rad $_{ABVS\ +\ 2D}$), the habitat radiomics model (Hab $_{ABVS\ +\ 2D}$), the combined radiomics model (Rad-Hab $_{ABVS\ +\ 2D}$), and the Clinical–Radiomics–Habitat $_{ABVS+2D}$ Combined Model(CM $_{Clinical\ +\ Rad\text{-}Hab}$). The entire model construction workflow is shown in Figure 2. All models were established using radiomics features derived from ABVS and 2D images. Four ML classifiers were employed: logistic regression (LR), ExtraTree (ET), EXtreme Gradient Boosting (XGBoost), and Light Gradient Boosting Machine (LightGBM). To reduce overfitting, 5-fold cross-validation was applied within the training cohort to optimize hyperparameters for each classifier. Model performance was evaluated by plotting receiver operating characteristic (ROC) curves and calculating the area under the curve (AUC). The DeLong test was applied to statistically compare ROC performance across different models, while the Hosmer-Lemeshow test assessed the models' goodness-of-fit. Clinical utility was further evaluated using the DCA to estimate the net benefit of each model in guiding clinical decision-making.

Statistical Analysis

All statistical analyses and data visualizations were performed using R software (version 4.4.2) and JD_DCPM (V6.03, Jingding Medical Technology Co., Ltd.) and Python (version 3.8; https://www.python.org). Continuous variables were presented as mean ± standard deviation, while categorical variables were expressed as counts (n) and percentages (%). For quantitative data following a normal distribution, Student's *t*-test was used. Levene's test was employed to assess the

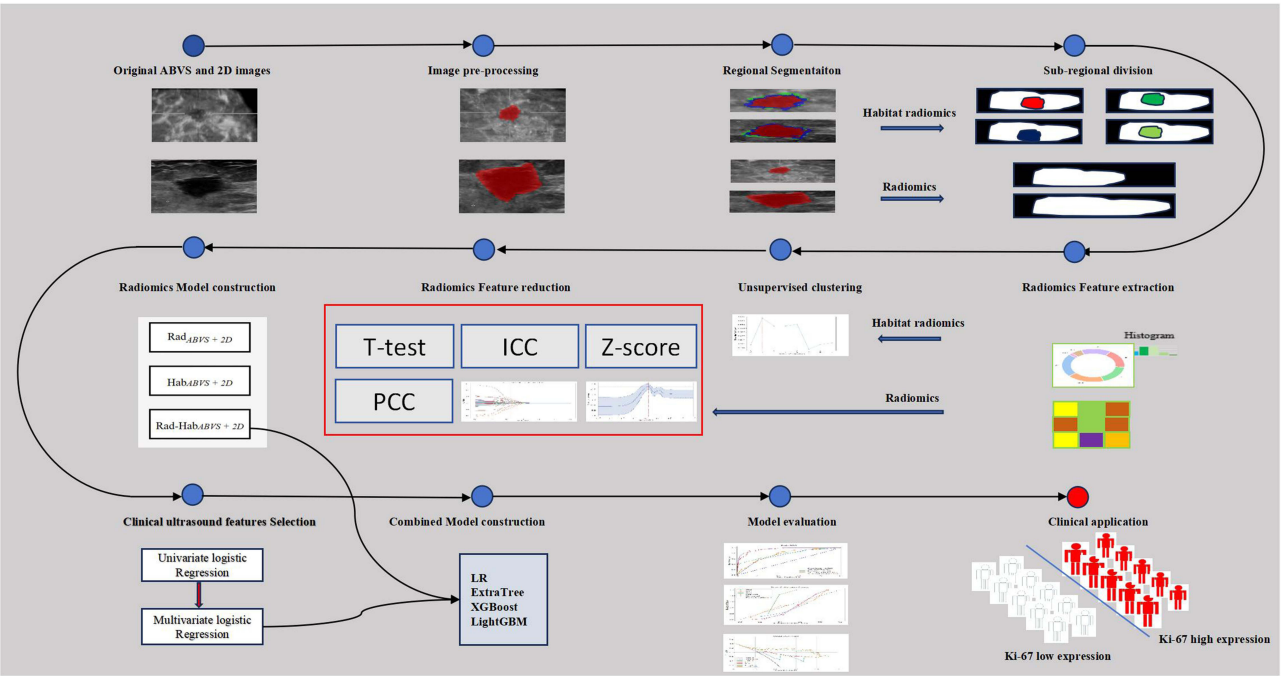

Figure 2 Workflow of radiomics analysis. This figure illustrates the segmentation, feature extraction, and feature selection process for ABVS and 2D images in breast cancer. **Abbreviations**: ABVS, automated breast volume scanner; ICC, intraclass correlation coefficient; LASSO, least absolute shrinkage and selection operator; PCC, Pearson correlation coefficient; Rad$_{ABVS+2D}$, Radiomics ABVS and 2D model; Had$_{ABVS+2D}$, Habitat radiomics ABVS and 2D model; Rad-Hab$_{ABVS+2D}$, Radiomics and Habitat radiomics ABVS and 2D model; CM$_{Clinical\ +\ Rad\text{-}Hab}$, Clinical–Radiomics–Habitat $_{ABVS+2D}$ Combined Model.

https://doi.org/10.2147/BCTT.S540595

homogeneity of variance. The Kruskal–Wallis test was used for non-normally distributed data. The Chi-square test was applied to compare categorical data. The DeLong test was used to compare the ROC performance among different models. All statistical tests were two-sided, and statistical significance was set at $P < 0.05$.

Results

Comparison of Baseline Data

A total of 426 eligible BC patients were included in this study, with 297 patients assigned to the training set and 129 to the validation set. A summary of baseline clinical and US characteristics is presented in Table 1. Among these variables, multivariate logistic regression analysis identified T-stage and US-ALNs as independent predictors. These two factors were therefore incorporated into the clinical model (Table 2). Using LR, the clinical model achieved an AUC of 0.720 (95% CI: 0.662–0.775) in the training set and 0.648 (95% CI: 0.557–0.734) in the validation set.

Table 1 Baseline Clinical Ultrasound Characteristics in the Training and Validation Sets

Characteristics	Training Set (N=297)			Validation Set (N=129)		
	Ki-67 High Expression (N=206)	*Ki-67* Low Expression (N=91)	*P*	*Ki-67* High Expression (N=86)	*Ki-67* Low Expression (N=43)	*P*
Age	54.01±10.43	54.47±9.88	0.718	53.56±12.31	54.98±10.24	0.490
T-stage			<0.001			0.093
≤2.0cm	61	54		37	26	
>2cm	145	37		49	17	
Side			0.956			0.574
Left	111	48		48	21	
Right	95	43		38	22	
Shape			0.875			0.423
Regular	11	6		6	1	
Irregular	195	85		80	42	
Orientation			0.223			0.300
Parallel	186	77		38	81	
Non-parallel	20	14		5	5	
Margin			0.332			1.000
Circumscribed	14	10		7	3	
Non-circumscribed	192	81		79	40	
PEF			0.955			0.154
No change	163	71		28	67	
Enhance	16	8		4	9	
Attenuation	27	12		11	10	
Calcification			0.214			0.842
Absent	135	67		30	57	
Present	71	24		13	29	
RPS			0.082			0.493
No	128	46		24	41	
YES	78	45		19	45	
BI-RADS			0.028			0.679
3	2	4		2	0	
4a	17	15		10	6	
4b	59	21		20	14	
4c	78	33		31	12	
5	50	18		23	11	

(*Continued*)

Table 1 (Continued).

Characteristics	Training Set (N=297)			Validation Set (N=129)		
	Ki-67 High Expression (N=206)	*Ki-67* Low Expression (N=91)	*P*	*Ki-67* High Expression (N=86)	*Ki-67* Low Expression (N=43)	*P*
US-ALNs			<0.001			0.030
Negative	135	83		57	37	
Positive	71	8		29	6	
Histological.type			0.244			0.597
IDC	187	76		79	38	
DCIS	8	5		2	3	
ILC	2	2		1	0	
Others	9	8		4	2	

Abbreviations: PEF, posterior echo feature; RPS, retraction phenomenon sign; US-ALNs, ultrasound-based axillary lymph node status; BI-RADS, Breast Imaging Reporting and Data System; IDC, invasive ductal carcinoma; DCIS, ductal carcinoma in situ; ILC, invasive lobular carcinoma.

Table 2 Univariate and Multivariate Logistic Regression Analyses of Clinical Ultrasound Characteristics in the Training Set

Characteristics	Univariate Analysis OR (95% CI)	*P*	Multivariate Analysis OR (95% CI)	*P*
Age	0.996(0.972–1.020)	0.722		
T-stage	3.469(2.084–5.840)	<0.001	3.078 (1.818–5.265)	<0.001
Side	0.955(0.583–1.569)	0.856		
Shape	1.251(0.419–3.401)	0.669		
Orientation	0.591(0.286–1.252)	0.160		
Margin	1.693(0.703–3.943)	0.226		
PEF				
No-change	Reference			
Enhance	0.871(0.365–2.234)	0.762		
Attenuation	0.980(0.479–2.108)	0.957		
Calcification	1.468(0.857–2.573)	0.169		
RPS	0.623(0.378–1.025)	0.063		
BI-RADS				
3	Reference			
4a	2.267(0.385–18.07)	0.382		
4b	5.619(1.021–42.71)	0.056		
4c	4.727(0.879–35.31)	0.081		
5	5.556(0.998–42.61)	0.059		
US-ALNs	5.456(2.637–12.80)	<0.001	4.759 (2.260–11.30)	<0.001
Histological type				
IDC	Reference			
DCIS	0.650(0.21–2.21)	0.463		
ILC	0.406(0.048–3.437)	0.372		
Others	0.457(0.169–1.26)	0.121		

Abbreviations: PEF, posterior echo feature; RPS, retraction phenomenon sign; US-ALNs, ultrasound-based axillary lymph node status; BI-RADS, Breast Imaging Reporting and Data System; IDC, invasive ductal carcinoma; DCIS, ductal carcinoma in situ; ILC, invasive lobular carcinoma.

https://doi.org/10.2147/BCTT.S540595

Screening of Radiomics Features

Rad $_{ABVS + 2D}$ Feature Selection

In the training set, the tumor ROI were delineated on both ABVS and 2D US images, and a total of 464 radiomics features were extracted from each image. After standardization, features with an intraclass correlation coefficient (ICC) > 0.75 were retained for subsequent analysis, resulting in 898 features. Subsequently, univariate *t*-tests and Pearson correlation coefficient (PCC) analyses were conducted to evaluate the relationships among these features. Finally, the least absolute shrinkage and selection operator (LASSO) algorithm was used to select the most predictive features based on the optimal λ value. The Rad $_{ABVS + 2D}$ model identified 15 radiomics features, 9 from ABVS images and 6 from 2D US images, that were significantly correlated with *Ki-67* expression (λ=0.037, Figure S1).

Hab $_{ABVS + 2D}$ Feature Selection

In this study, the Silhouette Coefficient was used to evaluate clustering performance and determine the optimal number of clusters (Figure 3A). The analysis revealed that when the number of clusters was set to 3, the silhouette coefficient reached its highest value, indicating the best clustering performance. Accordingly, the tumor ROI was divided into three habitat sub-regions for subsequent feature extraction and model construction. For each sub-region, 464 radiomics features were extracted, resulting in a total of 2694 features (898 features × 3 sub-regions), following intraclass correlation coefficient (ICC) filtering. Feature selection was then conducted, and the final Hab $_{ABVS + 2D}$ model identified 13 ABVS and 12 2D radiomics features that were significantly correlated with *Ki-67* expression (λ=0.018, Figure S2). The habitat feature maps and corresponding sub-region segmentations are shown in Figure 3B and C.

Rad-Hab $_{ABVS + 2D}$ Feature Selection

According to the methodology described above, the Rad-Hab $_{ABVS + 2D}$ model initially included a total of 3592 features (898 + 898×3). After feature selection and dimensionality reduction, the final model identified 16 ABVS features and 8 2D radiomics features that were significantly correlated with *Ki-67* expression (λ=0.012, Figure S3).

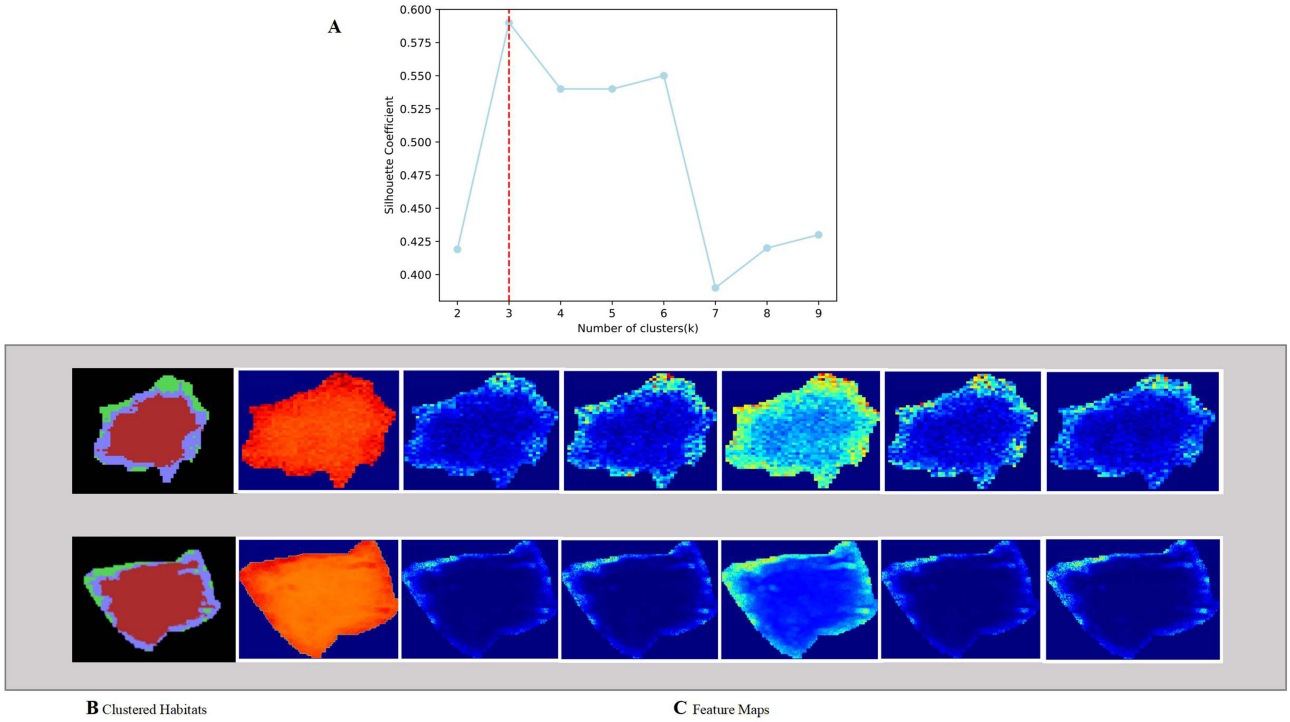

Figure 3 Determination of optimal clusters and visualization of habitat clusters with corresponding feature maps. (**A**) Silhouette coefficient plot was used to determine the optimal number of clusters (k), indicating that k=3 is optimal. (**B**) Distribution of habitats under different clustering numbers, with different colors representing different clusters. (**C**) Feature maps for the following parameters: original_glcm_DifferenceVariance, original_glcm_Idm, original_glcm_InverseVariance, original_glcm_JointAverage, original_glcm_JointEnergy, original_glcm_MaximumProbability.

Construction and Validation of Each Models

The optimal model for the traditional Rad $_{ABVS + 2D}$ configuration was LR, as detailed in Table S1 and Figure S4A and B. In the training set, the model achieved an AUC of 0.755 (95% CI: 0.688–0.813), with accuracy, sensitivity, specificity, and F1-score of 0.670, 0.824, 0.602, and 0.605, respectively. In the internal validation set, the AUC was 0.603 (95% CI: 0.515–0.690), with corresponding values of 0.682 for accuracy, 0.442 for sensitivity, 0.802 for specificity, and 0.481 for F1-score.

For the Hab $_{ABVS + 2D}$ model, the best-performing algorithm was ExtraTree, as detailed in Table S2 and Figure S4C and D). In the training set, the model achieved an AUC of 0.779 (95% CI: 0.712 −0.825), with accuracy, sensitivity, specificity, and F1-score of 0.781, 0.505, 0.903, and 0.586. In the validation set, the AUC was 0.664 (95% CI: 0.579–0.755), and accuracy, sensitivity, specificity, and F1-score were 0.605, 0.721, 0.547, and 0.549, respectively.

The Rad-Hab $_{ABVS + 2D}$ model performed best when using the XGBoost, as detailed in Table S3 and Figure S4E and F. In the training set, the model achieved an AUC of 0.935 (95% CI: 0.910–0.962), with accuracy, sensitivity, specificity, and F1-score of 0.869, 0.868, 0.869, and 0.802, respectively. In the validation set, the AUC was 0.850 (95% CI: 0.789–0.918), with values of 0.806 for accuracy, 0.744 for sensitivity, 0.837 for specificity, and 0.719 for F1-score.

After combining Rad-Hab$_{ABVS + 2D}$ features with clinical features, the ML model achieving the best performance was based on LightGBM, as detailed in Table S4 and Figure S4G and H. This resulting model was designated CM $_{Clinical + Rad\text{-}Hab}$. In the training set, the model achieved an AUC of 0.951 (95% CI: 0.928–0.973), with accuracy, sensitivity, specificity, and F1-score of 0.886, 0.890, 0.883, and 0.827, respectively. In the validation set, the AUC was 0.884 (95% CI: 0.831–0.949), with corresponding values of 0.783 for accuracy, 0.860 for sensitivity, 0.744 for specificity, and 0.725 for F1-score. Across the radiomics-based models, statistically significant differences in *Ki-67* expression were observed between the high- and low-expression groups, with the exception of the Rad $_{ABVS + 2D}$ in the validation set (P <0.01, Figure 4). The differences in radiomics features from specific habitat sub-regions included in the CM $_{Clinical + Rad\text{-}Hab}$ model are shown in Figure 5.

Comparison of Model Performance

In the training set, the DeLong test results indicated that the AUC differences between the CM $_{Clinical + Rad\text{-}Hab}$ model and the Clinical, Rad $_{ABVS + 2D}$, Hab $_{ABVS + 2D}$, and Rad-Hab $_{ABVS + 2D}$ models were all statistically significant (Z = 7.979, P < 0.001; Z = 7.162, P < 0.001; Z = 6.017, P < 0.001; Z = 2.669, P = 0.007). Similar results were observed in the validation set (Z = 4.829, P < 0.001; Z = 5.665, P < 0.001; Z = 4.885, P < 0.001; Z = 2.662, P = 0.009). These findings indicate that the CM $_{Clinical + Rad\text{-}Hab}$ model significantly outperformed the other models in predicting *Ki-67* expression, as presented in Figure 6A and B, Table 3. The calibration curves of the CM $_{Clinical + Rad\text{-}Hab}$ model exhibited strong agreement between expected and observed outcomes in both the high and low *Ki-67* expression groups, surpassing the calibration performance of the other models, as illustrated in Figure 6C and D. The Hosmer-Lemeshow test further confirmed good model calibration for the CM $_{Clinical + Rad\text{-}Hab}$ model, with P = 0.645 and 0.587 for the two sets.

The DCA demonstrated that CM $_{Clinical + Rad\text{-}Hab}$ achieved superior net clinical benefit compared to all- or no-treatment strategies, as shown in Figure 6E and F. Furthermore, incorporating the Rad-Hab $_{ABVS + 2D}$ model with clinical risk factors (T-stage, US-ALNs) significantly improved the predictive performance of the CM $_{Clinical + Rad\text{-}Hab}$. This improvement was confirmed by significant increases in both the net reclassification improvement (NRI) and integrated discrimination improvement (IDI) indicators in the training and validation sets (Table 4). NRI and IDI values for the other models can be found in Table S5.

Discussion

In this study, we proposed a new approach that integrates ABVS- and 2D-based lesion imaging with radiomics and habitat radiomics to predict the expression of *Ki-67* in BC. Our results demonstrated that the Rad-Hab $_{ABVS+2D}$ model could accurately predict *Ki-67* expression, and that incorporating clinical factors into this model (CM $_{Clinical + Rad\text{-}Hab}$) further enhanced predictive performance. This approach provides a new strategy for constructing *Ki-67* prediction models in BC. More importantly, by leveraging ML to integrate radiomics features, our approach addresses tumor heterogeneity and enables complex nonlinear feature interpretation, thereby improving predictive accuracy.

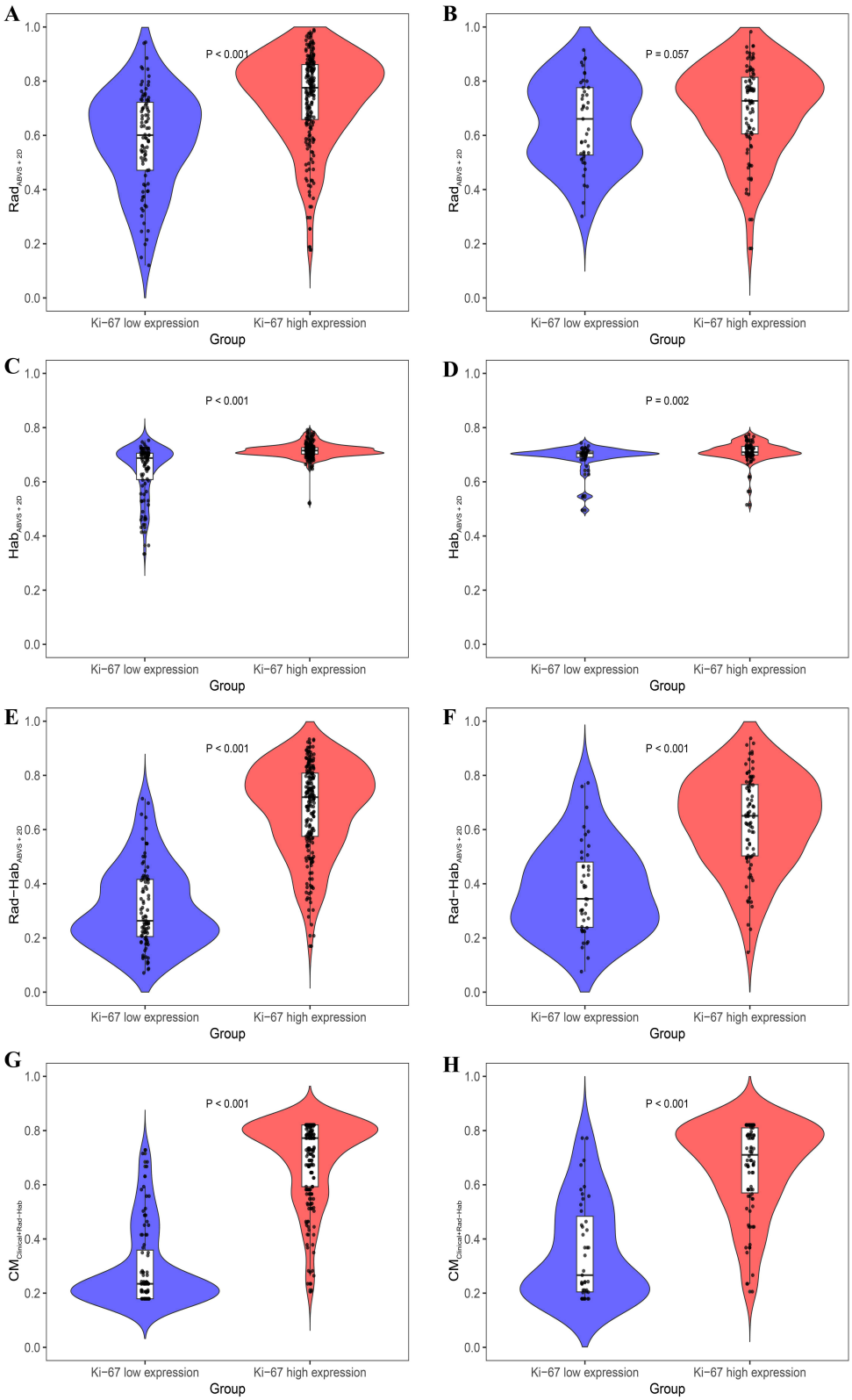

Figure 4 Comparison of the performance of different radiomics models in the training and validation sets. This figure shows the distribution of radiomics model outputs between the high- and low-expression *Ki-67* groups. (**A** and **B**) $Rad_{ABVS+2D}$; (**C** and **D**) $Hab_{ABVS+2D}$; (**E** and **F**) $Rad\text{-}Hab_{ABVS+2D}$; (**G** and **H**) $CM_{Clinical\ +\ Rad\text{-}Hab}$.
Abbrteviations: $Rad_{ABVS+2D}$, Radiomics ABVS and 2D model; $Had_{ABVS+2D}$, Habitat radiomics ABVS and 2D model; $Rad\text{-}Hab_{ABVS+2D}$, Radiomics and Habitat radiomics ABVS and 2D model; $CM_{Clinical\ +\ Rad\text{-}Hab}$, Clinical–Radiomics–Habitat $_{ABVS+2D}$ Combined Model; ABVS, automated breast volume scanner.

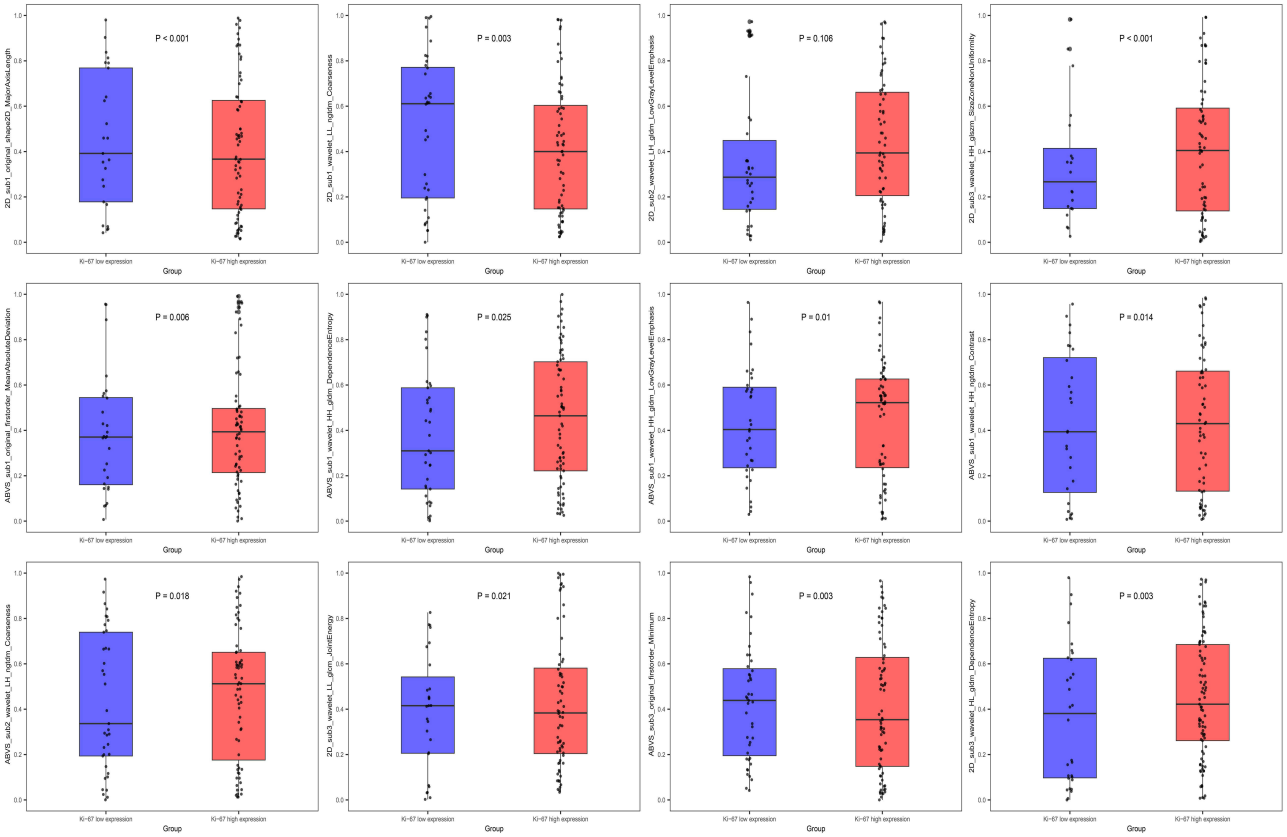

Figure 5 Box plot showing differences in ABVS and 2D image habitat radiomics features between the low- and high-expression groups in the $CM_{Clinical+Rad\_Hab}$ model. The *P* value indicates statistical significance and is displayed in each feature chart. Black dots represent individual data points; the horizontal line within each box indicates the median (50th percentile), and the upper and lower edges represent the 25th and 75th percentiles, respectively.
Abbreviation: ABVS, automated breast volume scanner.

A previous study utilized six ML algorithms to integrate US radiomics with postoperative pathological features to predict *Ki-67* expression in breast malignancies, reporting that the LR achieved the best average predictive performance (training AUC: 0.793, validation AUC: 0.798).[17] Another similar study also attempted to predict *Ki-67* expression, but the predictive performance was only moderate.[27] In our study, the $Rad\text{-}Hab_{ABVS\ +\ 2D}$ model achieved AUC values of 0.935 in the training cohort and 0.850 in the validation cohort, demonstrating strong predictive capability. Furthermore, by integrating US features (US-ALNs and T-stage), the LightGBM-based $CM_{Clinical\ +\ Rad\text{-}Hab}$ model achieved even higher performance (training AUC: 0.951, validation AUC: 0.884). The calibration curve demonstrated excellent predictive accuracy, while DCA showed good clinical benefits. These findings highlight the potential of ML-based multimodal radiomics as a non-invasive tool for personalized clinical diagnosis and treatment planning.

Radiomics has emerged as a specialized field within medical imaging, enabling the extraction of high-throughput quantitative features from medical images. This approach captures the intrinsic characteristics of breast tumors, and to some extent, provides additional insights into *Ki-67* expression in BC.[28] By applying various ML or deep learning algorithms to different imaging modalities,[2,11,27] key information about *Ki-67* expression in BC can be obtained, supplementing conventional pathological assessments. In our study, dimensionality reduction of the $Rad\text{-}Hab_{ABVS\ +\ 2D}$ model yielded 24 key radiomics features related to the *Ki-67* status. These features, combined with clinical variables, were evaluated using four ML algorithms (LR, ET, XGBoost, and LightGBM). The results showed that LightGBM demonstrated the best predictive performance. As a gradient boosting decision tree algorithm, LightGBM enhances performance by increasing the number of boosting trees and offers efficiency and flexibility in modeling nonlinear relationships. Its ability to handle large datasets with high-dimensional features makes it particularly effective for

https://doi.org/10.2147/BCTT.S540595

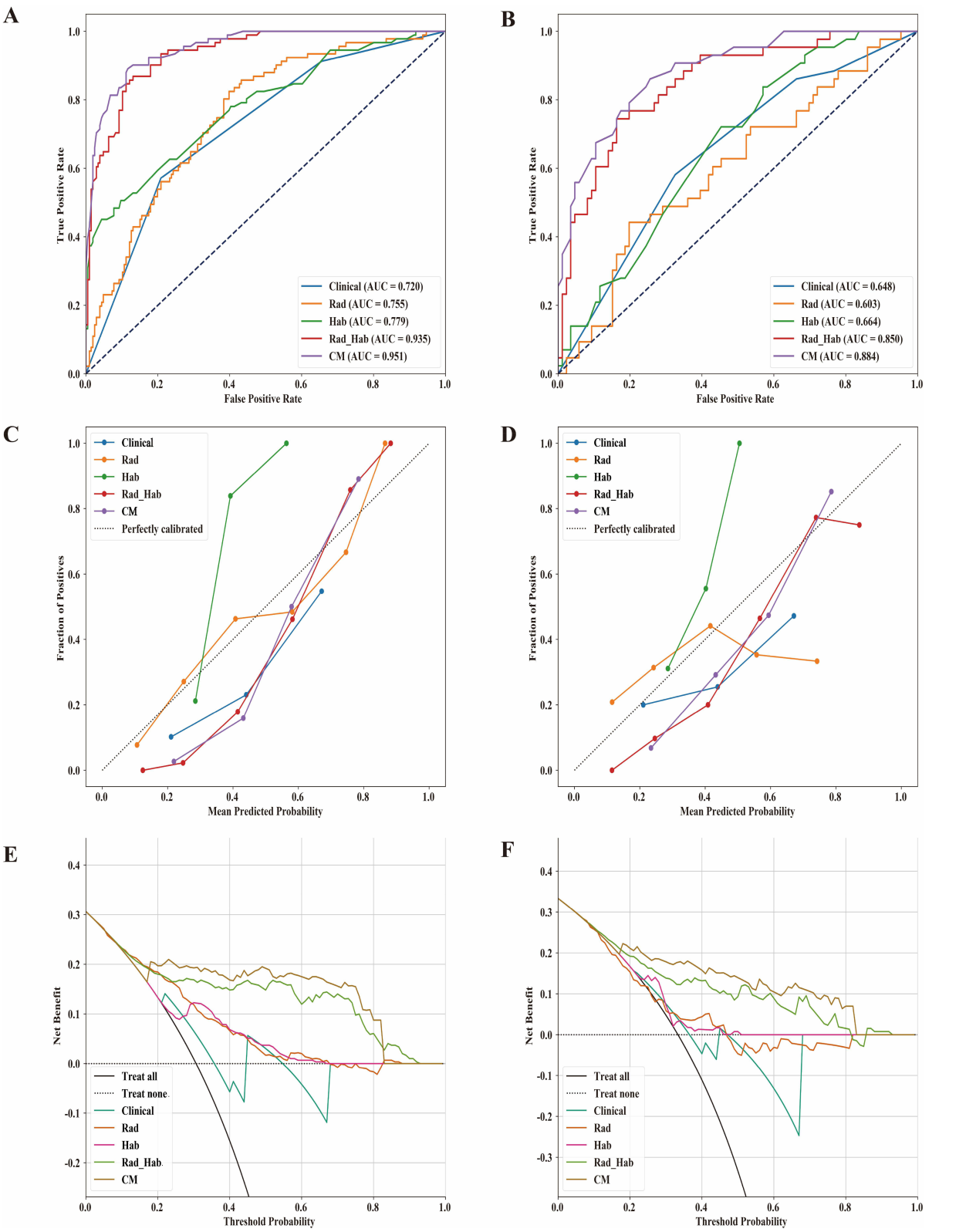

Figure 6 ROC curves (**A** and **B**), calibration curves (**C** and **D**), and DCA curves (**E** and **F**) for different models in the training and validation sets.
Abbreviations: DCA, Decision Curve Analysis; ROC, Receiver Operating Characteristic; ABVS, automated breast volume scanner; $Rad_{ABVS+2D}$, Radiomics ABVS and 2D model; $Had_{ABVS+2D}$, Habitat radiomics ABVS and 2D model; $Rad\text{-}Hab_{ABVS+2D}$, Radiomics and Habitat radiomics ABVS and 2D model; CM $_{Clinical\ +\ Rad\text{-}Hab}$, Clinical–Radiomics–Habitat $_{ABVS+2D}$ Combined Model.

https://doi.org/10.2147/BCTT.S540595

Table 3 Comparison of Radiomics and Sub-Region Features Across Different Models Using ABVS and 2D Imaging

Group	Model	Accuracy	AUC	95% CI	Sensitivity	Specificity	PPV	NPV	F1
Training	Clinical	0.723	0.720	0.662–0.775	0.571	0.791	0.547	0.559	0.559
	$Rad_{ABVS+2D}$	0.670	0.755	0.688–0.813	0.824	0.602	0.478	0.885	0.605
	$Hab_{ABVS+2D}$	0.781	0.779	0.688–0.813	0.505	0.903	0.697	0.805	0.585
	$Rad\text{-}Hab_{ABVS+2D}$	0.868	0.935	0.711–0.825	0.868	0.869	0.745	0.937	0.802
	$CM_{Clinical+Rad\text{-}Hab}$	0.885	0.951	0.910–0.962	0.890	0.883	0.771	0.948	0.826
Validation	Clinical	0.643	0.648	0.557–0.734	0.581	0.674	0.471	0.763	0.520
	$Rad_{ABVS+2D}$	0.682	0.603	0.515–0.699	0.442	0.802	0.528	0.742	0.481
	$Hab_{ABVS+2D}$	0.605	0.664	0.579–0.755	0.720	0.547	0.696	0.867	0.549
	$Rad\text{-}Hab_{ABVS+2D}$	0.806	0.850	0.789–0.918	0.744	0.837	0.696	0.867	0.719
	$CM_{Clinical+Rad\text{-}Hab}$	0.782	0.884	0.831–0.949	0.860	0.744	0.627	0.914	0.725

Abbreviations: AUC, area under the curve; CI, confidence interval; NPV, negative predictive value; PPV, positive predictive value, F1, F1 score; $Rad_{ABVS+2D}$, Radiomics ABVS and 2D model; $Had_{ABVS+2D}$, Habitat radiomics ABVS and 2D model; $Rad\text{-}Hab_{ABVS+2D}$, Radiomics and Habitat radiomics ABVS and 2D model; CM $_{Clinical\ +\ Rad\text{-}Hab}$, Clinical–Radiomics–Habitat $_{ABVS+2D}$ Combined Model.

Table 4 Evaluation of CM $_{\text{Clinical + Rad-Hab}}$ and Clinical Models Using NRI and IDI

	Training set			Validation Set		
	Categorical NRI	Continuous NRI	IDI	Categorical NRI	Continuous NRI	IDI
CM $_{Clinical\ +\ Rad\text{-}Hab}$ VS Clinical	1.086 (0.953–1.218)	1.276 (1.086–1.468)	0.274	0.826 (0.602–1.049)	0.884 (0.551–1.217)	0.219
P	<0.001	<0.001	<0.001	<0.001	<0.001	<0.001

Abbreviations: NRI, net reclassification improvement; IDI, integrated discrimination improvement; CM $_{Clinical\ +\ Rad\text{-}Hab}$, Clinical–Radiomics–Habitat $_{ABVS+2D}$ Combined Model.

predictive modeling.[29] Numerous studies have confirmed the robustness and reliability of LightGBM in classification and regression tasks,[29–31] further proving its robustness and reliability as a powerful classification tool.

The results of this study indicated that, within our developed CM $_{Clinical\ +\ Rad\text{-}Hab}$ model, the Rad-Hab $_{ABVS\ +\ 2D}$ component was the most influential predictive factor. Tumors represent complex ecosystems, and intratumoral heterogeneity is often distributed unevenly throughout the lesion.[32] However, regional heterogeneity within the tumor is frequently overlooked. Recent studies have shown that voxels at different spatial locations within an image may share similar imaging features, and these sub-regions may exhibit comparable biological characteristics.[33] Therefore, to better study and quantify such regional heterogeneity, habitat radiomics divides tumors into sub-regions consisting of voxel clusters with similar characteristics for unsupervised analysis.[34] Recently, this approach has achieved promising results in the assessment of parotid gland tumors, liver cancer, and BC, among others.[3,32,35] In our $CM_{Clinical+Rad\text{-}Hab}$ model, it is noteworthy that most of the 24 selected radiomics features were derived from wavelet features (16 features). These wavelet features effectively capture heterogeneity at multiple spatial scales (Figure S3),[36] patterns that are typically imperceptible through visual inspection but can be extracted using radiomics and mathematically correlated with the *Ki-67* status. Although the $Rad\_Hab_{ABVS+2D}$ model alone demonstrated strong predictive performance, incorporating clinical parameters (T-stage, OR = 3.078; US-ALNs, OR = 4.759) significantly improved the overall performance of the $CM_{Clinical+ABVS+2D}$ model (training set: Z = 2.669, *P* = 0.007; validation set: Z = 2.662, *P* = 0.009). This observation result is consistent with the studies,[9,11,37] emphasizing that only by fully leveraging multi-dimensional data can the radiomics features reach their full potential in predicting *Ki-67* expression (Table 3 and Figure 6).

Although previous studies have used either ABVS or 2D single-modality images to predict *Ki-67* expression, to our knowledge, this study is the first to integrate radiomics features from both ABVS and 2D US images, including sub-regional (habitat) features, for *Ki-67* prediction. However, several limitations should be noted. First, as a single-center retrospective study, potential selection bias may limit the generalizability of the findings; future multicenter, prospective studies are needed to address this issue. Second, while this study is the first to employ multimodal sub-region radiomics

analysis for *Ki-67* prediction, model interpretability remains challenging due to the complexity of habitat radiomics, and incorporating explainable AI techniques could improve clinical interpretability. Third, our study was restricted to ABVS and 2D US images, excluding other modalities such as mammography and MRI, which could provide complementary diagnostic information; integrating these modalities in future studies may further enhance model performance. Lastly, radiomics features were extracted only from ABVS coronal images and the maximum 2D tumor section; extending analyses to 3D imaging or multiple planes may provide a more comprehensive characterization of tumor heterogeneity. In the future, we plan to explore correlations between radiomics or deep learning features and biomarkers such as *Ki-67* and HER-2 expression, as well as treatment responses to NAT, using multimodal imaging, to provide deeper insights for the precise treatment of BC.

Conclusion

In conclusion, this study demonstrates that integrating ML with ABVS and 2D US tumor- and sub-regional-based radiomics features can effectively predict *Ki-67* expression in BC. The developed $CM_{Clinical\ +\ Rad\text{-}Hab}$ model, which combines US indicators with radiomics features, achieves excellent classification performance and shows substantial clinical value. This approach holds significant potential for improving preoperative diagnostic accuracy and facilitating therapeutic efficacy assessment of BC biomarkers.

Ethics Statement

This retrospective study was approved by the Ethics Committee of the First Affiliated Hospital of Anhui Medical University, with a waiver of informed consent. All research data were de-identified and processed in strict accordance with relevant privacy protection regulations to ensure the confidentiality of participant information.

Acknowledgments

We sincerely acknowledge all the staff involved in implementing the intervention and assessing the research components. We also acknowledge the PixelMed AI platform and its developers for their valuable assistance with the code used in this revised manuscript.

Funding

This study was supported by Anhui Provincial Natural Science Foundation (Grant number: 2308085MH278), Health Research Program of Anhui (Grant number: AHWJ2023A10017), Anhui Provincial Health Commission Scientific Research Project (Grant number: AHWJ2024Aa30096), and Scientific Research Foundation for High-level Talents of First Affiliated Hospital of Wannan Medical College (Grant number: YR202436).

Disclosure

The author declares no potential conflicts of interest with respect to the research, authorship, and publication of this article.

References

1. Sung H, Ferlay J, Siegel RL, et al. Global cancer statistics 2020: GLOBOCAN estimates of incidence and mortality worldwide for 36 cancers in 185 countries. *CA Cancer J Clin*. 2021;71(3):209–249. doi:10.3322/caac.21660
2. Li HE, Cheng C. Development and assessment of a predictive model for *Ki-67* expression using ultrasound indicators and non-morphological magnetic resonance imaging parameters before breast cancer therapy. *Ultrason Imaging*. 2024;46(6):332–341. doi:10.1177/01617346241271107
3. Yerushalmi R, Woods R, Ravdin PM, Hayes MM, Gelmon KA. Ki67 in breast cancer: prognostic and predictive potential. *Lancet Oncol*. 2010;11(2):174–183. doi:10.1016/S1470-2045(09)70262-1
4. Mukai H, Yamaguchi T, Takahashi M, et al. *Ki-67* response-guided preoperative chemotherapy for HER2-positive breast cancer: results of a randomised Phase 2 study. *Br J Cancer*. 2020;122(12):1747–1753. doi:10.1038/s41416-020-0815-9
5. Chen R, Ye Y, Yang C, et al. Assessment of the predictive role of pretreatment *Ki-67* and *Ki-67* changes in breast cancer patients receiving neoadjuvant chemotherapy according to the molecular classification: a retrospective study of 1010 patients. *Breast Cancer Res Treat*. 2018;170(1):35–43. doi:10.1007/s10549-018-4730-1

6. Smith I, Robertson J, Kilburn L, et al. Long-term outcome and prognostic value of Ki67 after perioperative endocrine therapy in postmenopausal women with hormone-sensitive early breast cancer (POETIC): an open-label, multicentre, parallel-group, randomised, Phase 3 trial. *Lancet Oncol*. 2020;21(11):1443–1454. doi:10.1016/S1470-2045(20)30458-7
7. Rossi C, Fraticelli S, Fanizza M, et al. Concordance of immunohistochemistry for predictive and prognostic factors in breast cancer between biopsy and surgical excision: a single-centre experience and review of the literature. *Breast Cancer Res Treat*. 2023;198(3):573–582. doi:10.1007/s10549-023-06872-9
8. Fang J, Zhao W, Li Q, Zhang B, Pu C, Wang H. Correlation analysis of conventional ultrasound characteristics and strain elastography with *Ki-67* status in breast cancer. *Ultrasound Med Biol*. 2020;46(11):2972–2978. doi:10.1016/j.ultrasmedbio.2020.06.024
9. Li F, Zhu TW, Lin M, et al. Enhancing *Ki-67* prediction in breast cancer: integrating intratumoral and peritumoral radiomics from automated breast ultrasound via machine learning. *Acad Radiol*. 2024;31(7):2663–2673. doi:10.1016/j.acra.2023.12.036
10. Vourtsis A. Three-dimensional automated breast ultrasound: technical aspects and first results. *Diagn Interv Imaging*. 2019;100(10):579–592. doi:10.1016/j.diii.2019.03.012
11. Wu Y, Ma Q, Fan L, Wu S, Wang J. An automated breast volume scanner-based intra- and peritumoral radiomics nomogram for the preoperative prediction of expression of *Ki-67* in breast malignancy. *Acad Radiol*. 2024;31(1):93–103. doi:10.1016/j.acra.2023.07.004
12. Lambin P, Rios-Velazquez E, Leijenaar R, et al. Radiomics: extracting more information from medical images using advanced feature analysis. *Eur J Cancer*. 2012;48(4):441–446. doi:10.1016/j.ejca.2011.11.036
13. Mayerhoefer ME, Materka A, Langs G, et al. Introduction to radiomics. *J Nucl Med*. 2020;61(4):488–495. doi:10.2967/jnumed.118.222893
14. Jiang W, Deng X, Zhu T, Fang J, Li J. ABVS-based radiomics for early predicting the efficacy of neoadjuvant chemotherapy in patients with breast cancers. *Breast Cancer*. 2023;15:625–636. doi:10.2147/BCTT.S418376
15. Ma Q, Shen C, Gao Y, et al. Radiomics analysis of breast lesions in combination with coronal plane of ABVS and strain elastography. *Breast Cancer*. 2023;15:381–390. doi:10.2147/BCTT.S410356
16. Wang SJ, Liu HQ, Yang T, et al. Automated Breast Volume Scanner (ABVS)-based radiomic nomogram: a potential tool for reducing unnecessary biopsies of BI-RADS 4 lesions. *Diagnostics*. 2022;12(1). doi:10.3390/diagnostics12010172
17. Wu J, Fang Q, Yao J, et al. Integration of ultrasound radiomics features and clinical factors: a nomogram model for identifying the *Ki-67* status in patients with breast carcinoma. *Front Oncol*. 2022;12:979358. doi:10.3389/fonc.2022.979358
18. Chen Y, Xie Y, Li B, et al. Automated Breast Ultrasound (ABUS)-based radiomics nomogram: an individualized tool for predicting axillary lymph node tumor burden in patients with early breast cancer. *BMC Cancer*. 2023;23(1):340. doi:10.1186/s12885-023-10743-3
19. Li J, Qiu Z, Zhang C, et al. ITHscore: comprehensive quantification of intra-tumor heterogeneity in NSCLC by multi-scale radiomic features. *Eur Radiol*. 2023;33(2):893–903. doi:10.1007/s00330-022-09055-0
20. Jardim-Perassi BV, Huang S, Dominguez-Viqueira W, et al. Multiparametric MRI and coregistered histology identify tumor habitats in breast cancer mouse models. *Cancer Res*. 2019;79(15):3952–3964. doi:10.1158/0008-5472.CAN-19-0213
21. Wu J, Li Y, Gong W, Li Q, Han X, Zhang T. Multi-modality radiomics diagnosis of breast cancer based on MRI, ultrasound and mammography. *BMC Med Imaging*. 2025;25(1):265. doi:10.1186/s12880-025-01767-1
22. D'Orsi C, Morris E, Mendelson E. ACR BI-RADS® Atlas, Breast Imaging Reporting and Data System. 2013:121–140.
23. Jiang M, Zhang D, Tang SC, et al. Deep learning with convolutional neural network in the assessment of breast cancer molecular subtypes based on US images: a multicenter retrospective study. *Eur Radiol*. 2021;31(6):3673–3682. doi:10.1007/s00330-020-07544-8
24. de Gregorio A, Friedl TWP, Hering E, et al. Ki67 as proliferative marker in patients with early breast cancer and its association with clinicopathological factors. *Oncology*. 2021;99(12):780–789. doi:10.1159/000517490
25. Zhang Y, Ma H, Lei P, Li Z, Yan Z, Wang X. Prediction of early postoperative recurrence of hepatocellular carcinoma by habitat analysis based on different sequence of contrast-enhanced CT. *Front Oncol*. 2024;14:1522501. doi:10.3389/fonc.2024.1522501
26. Zhang J, Wang X, Zhang L, et al. Radiomics predict postoperative survival of patients with primary liver cancer with different pathological types. *Ann Transl Med*. 2020;8(13):820. doi:10.21037/atm-19-4668
27. Zhu Y, Dou Y, Qin L, Wang H, Wen Z. Prediction of *Ki-67* of invasive ductal breast cancer based on ultrasound radiomics nomogram. *J Ultrasound Med*. 2023;42(3):649–664. doi:10.1002/jum.16061
28. Fan M, Liu Z, Xu M, et al. Generative adversarial network-based super-resolution of diffusion-weighted imaging: application to tumour radiomics in breast cancer. *NMR Biomed*. 2020;33(8):e4345. doi:10.1002/nbm.4345
29. Basha SM, Rajput DS, Vandhan V. Impact of gradient ascent and boosting algorithm in classification. *Int J Intell Eng Syst*. 2018;11(1):41–49. doi:10.22266/ijies2018.0228.05
30. Zhang J, Mucs D, Norinder U, Svensson F. LightGBM: an effective and scalable algorithm for prediction of chemical toxicity-application to the Tox21 and mutagenicity data sets. *J Chem Inf Model*. 2019;59(10):4150–4158. doi:10.1021/acs.jcim.9b00633
31. Yanagawa R, Iwadoh K, Akabane M, et al. LightGBM outperforms other machine learning techniques in predicting graft failure after liver transplantation: creation of a predictive model through large-scale analysis. *Clin Transplant*. 2024;38(4):e15316. doi:10.1111/ctr.15316
32. Ma Q, Wang J, Tu Z, et al. Prediction model of axillary lymph node status using an automated breast volume ultrasound radiomics nomogram in early breast cancer with negative axillary ultrasound. *Front Immunol*. 2025;16:1460673. doi:10.3389/fimmu.2025.1460673
33. O'Connor JP, Rose CJ, Waterton JC, Carano RA, Parker GJ, Jackson A. Imaging intratumor heterogeneity: role in therapy response, resistance, and clinical outcome. *Clin Cancer Res*. 2015;21(2):249–257. doi:10.1158/1078-0432.CCR-14-0990
34. Kim J, Ryu SY, Lee SH, Lee HY, Park H. Clustering approach to identify intratumour heterogeneity combining FDG PET and diffusion-weighted MRI in lung adenocarcinoma. *Eur Radiol*. 2019;29(1):468–475. doi:10.1007/s00330-018-5590-0
35. Xiao Y, Huang P, Zhang Y, et al. Component prediction in combined hepatocellular carcinoma-cholangiocarcinoma: habitat imaging and its biologic underpinnings. *Abdom Radiol*. 2024;49(4):1063–1073. doi:10.1007/s00261-023-04174-8
36. Xie C, Yang P, Zhang X, et al. Sub-region based radiomics analysis for survival prediction in oesophageal tumours treated by definitive concurrent chemoradiotherapy. *EBioMedicine*. 2019;44:289–297. doi:10.1016/j.ebiom.2019.05.023
37. Liu J, Wang X, Hu M, et al. Development of an ultrasound-based radiomics nomogram to preoperatively predict *Ki-67* expression level in patients with breast cancer. *Front Oncol*. 2022;12:963925. doi:10.3389/fonc.2022.963925

Breast Cancer: Targets and Therapy

Dovepress
Taylor & Francis Group

Publish your work in this journal

Breast Cancer - Targets and Therapy is an international, peer-reviewed open access journal focusing on breast cancer research, identification of therapeutic targets and the optimal use of preventative and integrated treatment interventions to achieve improved outcomes, enhanced survival and quality of life for the cancer patient. The manuscript management system is completely online and includes a very quick and fair peer-review system, which is all easy to use. Visit http://www.dovepress.com/testimonials.php to read real quotes from published authors.

Submit your manuscript here: https://www.dovepress.com/breast-cancer—targets-and-therapy-journal